Particle Physics at CERN

Annual Report 2008

(SNF grants 200020-115960 and 206620-119751)

E. Alagöz, Y. Allkofer, C. Amsler, A. Benelli, V. Boccone, V. Chiochia, W. Creus,
A. Dell'Antone, S. Horikawa, Hp. Meyer, B. Millan Mejias, P. Otyugova, C. Regenfus,
P. Robmann, J. Rochet, T. Rommerskirchen, A. Schmidt, S. Steiner,
D. Tsirigkas, and L. Wilke.

Secretariat: P. Perréard

April 9, 2009

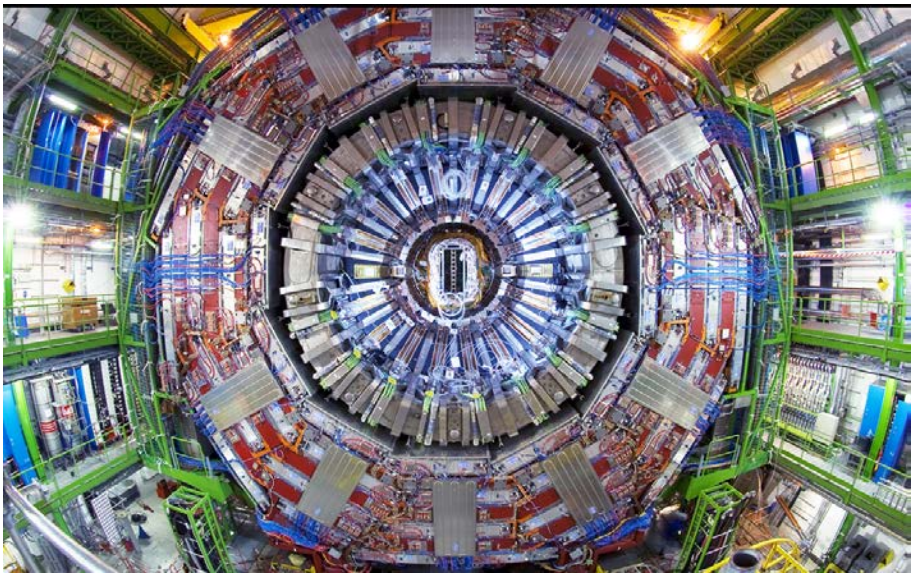

Physik-Institut der Universität Zürich
Winterthurerstrasse 190, CH-8057 Zürich, Switzerland

Contents

This report covers the activities of the Zurich group at CERN on the CMS, the DIRAC and the ArDM experiments between 1 April 2008 and 31 March 2009. It does not include the activity of one of us (C. A.) contributing to the "Review of Particle Physics" (Particle Data Group). Further details on the group activities and publication reprints can be obtained from our home page, see http://unizh.web.cern.ch/unizh/.

1 Evidence for πK-atoms

Y. Allkofer, C. Amsler, A. Benelli[1], S. Horikawa, C. Regenfus, and J. Rochet

In collaboration with:
CERN, Czech Technical University, Institute of Physics ACSR and Nuclear Physics Institute ASCR (Czech Republic), Laboratori Nazionali di Frascati, Messina University, Trieste University, KEK, Kyoto Sangyo University, Tokyo Metropolitan University, IFIN-HH (Bucharest), JINR (Dubna), Skobeltsin Institute for Nuclear Physics (Moscow), IHEP (Protvino), Santiago de Compostela University, Basel University, Bern University.

(DIRAC-II Collaboration)

Electromagnetically bound $\pi^{\mp}K^{\pm}$-pairs ($\pi^{\mp}K^{\pm}$-atoms) have been observed for the first time in 2008 by our DIRAC-II Collaboration at CERN [1, 2]. The π^+K^--atom is unstable and decays through the strong force into $\pi^0\bar{K}^0$ (while π^-K^+-atoms decay into π^0K^0). The mean life τ, which we intend to measure, is related to the S-wave πK-scattering lengths a_1 and a_3 in the isospin 1/2 and 3/2 states, respectively. The πK-scattering length is of interest to test chiral perturbation theories extended to the s-quark.

Predictions for τ can be obtained from the S-wave phase shifts of the πK-system, extrapolated to low energy kaon-nucleon scattering ($\pi K \to \pi K$ scattering off the exchanged π). However, kaon-nucleon scattering at low lomentum is difficult due to the short lifetime of the kaon and hence the S-phase shifts are poorly known at low energy. The experimental uncertainties in a_1 and a_3 are correspondingly substantial, and the predicted mean life of πK-atoms scatters between 1 and 5 fs. Using the values from dispersion relations [3] one predicts a mean life $\tau \sim 3.7$ fs.

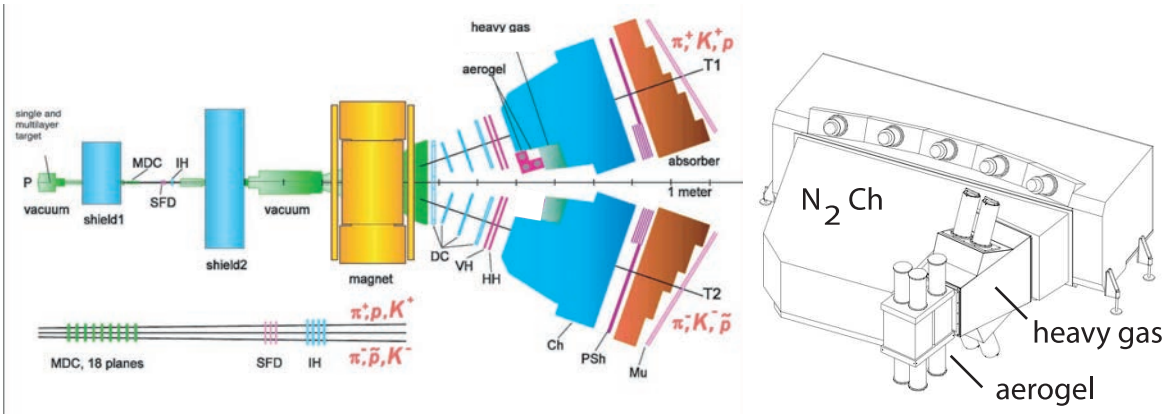

Figure 1.1: *Sketch of the updated DIRAC-II spectrometer, showing the locations of the Čerenkov counters to identify electrons, pions and kaons. MDC = microdrift chambers, SFD = scintillator fibre detector, IH = ionization hodoscope, DC = drift chambers, VH, HH = vertical and horizontal scintillation hodoscopes, PSh = preshower, Mu = muon counters. Right: N_2, aerogel and heavy gas Čerenkov counters.*

Details on the previous apparatus (DIRAC-I) to study $\pi^+\pi^-$-atoms [4] can be found in ref. [5]. A sketch of the modified spectrometer (DIRAC-II) to collect the πK (and more $\pi\pi$) data is shown in fig. 1.1. The 24 GeV/c proton beam from the CERN-PS impinges on a 26 μm Pt-target (average intensity of 1.6×10^{11} protons/pulse). The proton beam then passes through a vacuum pipe and

[1] Visitor from the University of Basel

is absorbed by the beam dump. The secondary particles emerging from the target are analyzed in a double-arm magnetic spectrometer measuring the momentum vectors of two oppositely charged hadrons. The particles are collimated through two steel shielding blocks, upstream of the microdrift chambers (MDC) and downstream of the ionization hodoscope (IH), respectively. They pass through a vacuum chamber and are bent by the 1.65 T field of the dipole magnet. The two-arm spectrometer is tilted upwards with respect to the proton beam by an angle of 5.7°. Positive particles are deflected into the left arm, negative ones into the right arm. Electrons and positrons are vetoed by the N_2-Čerenkov detectors and muons by their signals in scintillation counters behind the steel absorbers. Pions are separated from kaons with the heavy gas and aerogel counters. The signal from πK-atoms is observed for kaon and pion pairs with a very small relative momentum (typically $|Q_L| < 3$ MeV/c is the c.m.s system).

The Zurich group carries the main responsibility for the πK measurements, while the rest of the collaboration concentrates on $\pi\pi$. Our group has developed and built a novel aerogel Čerenkov counter in the left arm (positive charges) for kaon detection and proton suppression, and the heavy gas system for pion detection. An aerogel detector in the right arm (negative charges) is not necessary since the antiproton flux is negligible compared to that from negative kaons, while protons in the left arm are much more frequent than positive kaons. The aerogel detector consists of three independent modules. Two of them (total volume of 24ℓ) have refractive index $n = 1.015$ for kaons between 4 and 5.5 GeV/c, and the third one (13ℓ) has the lower index $n = 1.008$ for 5.5 to 8 GeV/c kaons and kaon-proton separation. The loss due to light absorption is compensated by using a wavelength shifter and by increasing the radiator thickness in the center of the detector (pyramid geometry). Details can be found in our recent publications [6, 7] and in previous annual reports.

The startup of DIRAC-II, originally planned for summer 2006, was postponed by one year due to repeated failures of a switching magnet in the CERN primary proton beam line. The defective magnet was successfully replaced in spring 2007 and DIRAC-II could be commissioned in June 2007. The aerogel counters worked according to expectations and data were taken in 2007 and 2008.

Last year the Zurich group was involved in the data analysis of the runs taken so far. This includes test beam calibrations and Monte-Carlo simulation for the aerogel counter. An event preselection was performed for both the πK and the $\pi\pi$ data. We studied the energy loss in the detector for the various particles and thereby cured a longstanding small momentum shift in the Q_L-distribution. We now describe the analysis of the 2007 data which led to the first observation of πK-atoms [1, 2].

For this analysis we used only detectors downstream of the dipole magnet. The trajectories were determined by the drift chambers, the pattern recognition starting from the coordinates in the last plane and extrapolating back to the target. The variable of interest in the following analysis is the relative momentum Q of the $\pi^{\mp}K^{\pm}$-pairs in their center-of-mass systems, in particular the longitudinal component Q_L which is not affected by multiple scattering. In the transverse plane, the resolution on the relative momentum Q_T (typically 3 MeV/c) is dominated by multiple scattering, while the resolution on the longitudinal component Q_L (< 1 MeV/c) is not affected. For further analysis we use therefore only Q_L.

Figure 1.2 shows the four mechanisms which contribute to the production of $\pi^{\pm}K^{\mp}$-pairs. Accidental pairs are due to particles produced on different nucleons (fig. 1.2a), non-Coulomb-pairs are associated with the production of long-lived intermediate states (fig. 1.2b). On the other hand, $\pi^{\pm}K^{\mp}$-pairs which interact electromagnetically form correlated Coulomb-pairs (fig. 1.2c), or atomic bound states (fig. 1.2d). The latter atoms, while traveling through the target, can either decay, be (de)-excited or break up into $\pi^{\pm}K^{\mp}$-pairs which emerge from the target with very low relative momentum.

For prompt pairs the time difference between the positive and negative spectrometer arm lies between –0.5 and 0.5 ns. Accidental pairs are first removed using the time information from the vertical

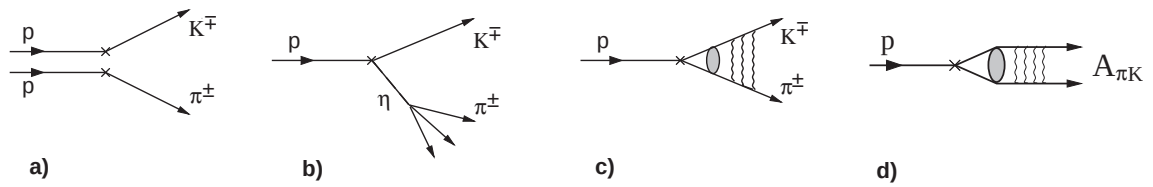

Figure 1.2: *Production mechanisms of πK-pairs: a) accidental-pairs from two protons; b) non-Coulomb-pairs from long-lived intermediate states such as the η-meson; c) Coulomb-pairs from direct production or from short-lived intermediate states; d) πK-atoms.*

hodoscopes. Accidental pairs (those with large time differences) are also needed for subsequent analysis. Electrons or muons are removed, and a loose preselection of oppositely charged particles is performed [2]. Pions, kaons and protons below 2.5 GeV/c can be separated by time-of-flight. For the $\pi^- K^+$ analysis the aerogel detector is used in addition to remove protons in the positive arm, while for the $\pi^+ K^-$ analysis the time difference between the negative and the positive arm has to be negative to remove protons faking pions.

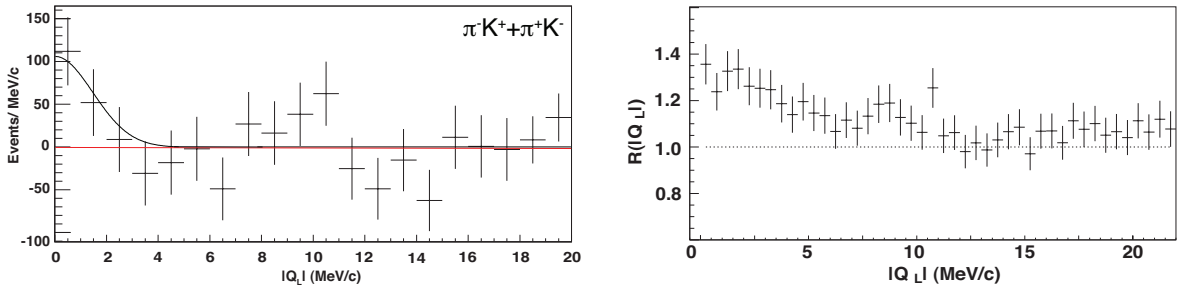

Figure 1.3: *Left: residuals between data and the fitted background for $\pi^- K^+$ and $\pi^+ K^-$. A Gaussian fit has been applied (solid line) to illustrate the distribution of atomic-pairs. Right: correlation function R as a function of $|Q_L|$ for πK-pairs. The deviation from the horizontal dotted line proves the existence of Coulomb-πK-pairs.*

Once the accidentals have been subtracted the prompt pairs are composed of the following three types: atomic-pairs, Coulomb-pairs, and non-Coulomb-pairs. We assume that the background due to non-Coulomb pairs can be described by the Q_L-distribution of accidentals, following a similar analysis for $\pi^+\pi^-$-atoms [4]. Coulomb pairs have to be simulated. Since the shapes of both contributions are known, one can extrapolate into the $|Q_L| < 3$ MeV/c signal region. The difference (residuals) between the data and the sum of both contributions is plotted in fig. 1.3 (left). Above $|Q_L| = 3$ MeV/c the residuals are consistent with zero, while the enhancement at low relative momentum is the first evidence for πK-atoms. We obtain 173 ± 54 detected atomic pairs with a statistical significance of 3.2σ. The systematic uncertainty is estimated to be around 5%, much smaller than the statistical one.

The evidence for the observation of πK-atoms is strengthened by the observation of Coulomb-pairs which, a fortiori, implies that atoms have also been produced. This can be seen as follows: non-Coulomb pairs have a similar Q_L-distribution as accidentals. Hence dividing the normalized distribution for prompt pairs by the one for accidentals one obtains the correlation function R describing Coulomb-pairs. The function R, shown in fig. 1.3 (right) as a function of $|Q_L|$, is clearly increasing with decreasing momentum, proving that Coulomb-pairs have been observed.

The ratio of the number of produced atoms to the number of Coulomb-pairs with small relative momenta has been calculated [8, 9]. This number needs to be corrected by Monte-Carlo simula-

tion to take into account the acceptance of the apparatus and the cuts applied in the analysis. The breakup probability P_{br} relates the number of atoms to the number of atomic pairs. A calculation of the breakup probability as a function of mean life (fig. 1.4) has been performed using the Born approximation [10]. For the predicted mean life of 3.7 fs P_{br} is 53% (dotted line in fig. 1.4). One then obtains from the number of produced atoms the predicted number of observed atomic pairs, 147 $\pm$ 36, in good agreement with the experimental result.

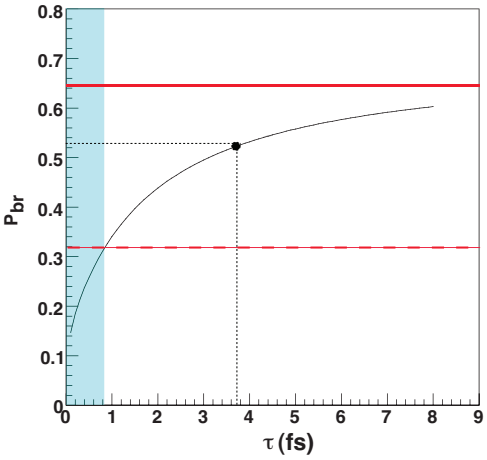

Figure 1.4: *Breakup probability P_{br} for the 26 μm Pt-target as a function of mean life of πK-atoms in the 1s-state. The horizontal solid line is the measured breakup probability and the horizontal dashed line the 1.28σ lower bound corresponding to a lower limit of 0.8 fs for the mean life. The excluded area (90% confidence level) is shown in blue. The horizontal dotted line gives the theoretical prediction corresponding to 3.7 fs.*

Conversely, one can use the number of observed atomic-pairs from the fit and the number of Coulomb-pairs below $|Q_L| < 3$ MeV/c to calculate the breakup probability: P_{br} = 64 $\pm$ 25 % (horizontal solid line in fig. 1.4). This leads to a lower limit for the mean life of πK-atoms of τ_{1S} = 0.8 fs at a confidence level of 90%. This result can be translated into an upper limit $|a_{1/2} - a_{3/2}| < 0.58$ m_π^{-1} at 90% confidence level.

The choice of Pt as production target for the 2007 data was justified by the high breakup probability so that of πK-atoms could be observed. Data taken in 2008 – 2010 are being collected with a 98 μm Ni-target, for which the breakup probability is lower ($\sim$35% according to ref. [10]) but still rapidly rising around the predicted mean life of 3.7 fs. This will allow a more accurate measurement of τ. The ultimate goal is to measure the mean life of πK-atoms with a precision of about 20%, leading to a 10% uncertainty in the difference of scattering lengths $|a_{1/2} - a_{3/2}|$.

References

[1] B. Adeva *et al.* (DIRAC Collaboration), Phys. Lett. **B 674** (2009) 11
[2] Y. Allkofer, PhD Thesis, University of Zurich (2008)
[3] P. Büttiker, S. Descotes-Genon, B. Moussallam, Eur. Phys. J. **C 33** (2004) 409
[4] B. Adeva *et al.* (DIRAC Collaboration), Phys. Lett. **B 619** (2005) 50
[5] B. Adeva *et al.* (DIRAC Collaboration), Nucl. Instrum. Methods in Phys. Res. **A 515** (2003) 467
[6] Y. Allkofer *et al.*, Nucl. Instr. Meth. in Phys. Research **A 582** (2007) 497;
Y. Allkofer *et al.*, Nucl. Instr. Meth. in Phys. Res. **A 595** (2008) 84
[7] S. Horikawa *et al.*, Nucl. Instr. Meth. in Phys. Res. **A 595** (2008) 212
[8] L.L. Nemenov, Sov. J. Nucl. Phys. **41** (1985) 629
[9] L. Afanasyev and O. Voskresenskaya, Phys. Lett. **B 453** (1999) 302
[10] B. Adeva et al., CERN-SPSC-2004-009, SPSC-P-284, Add.4

2 Particle physics with CMS

E. Alagöz, C. Amsler, V. Chiochia, Hp. Meyer, B. Millan Mejias, C. Regenfus, P. Robmann,
J. Rochet, T. Rommerskirchen, A. Schmidt, S. Steiner, D. Tsirigkas, and L. Wilke

In collaboration with:
Paul Scherrer Institut (PSI) and the CMS Collaboration

The silicon pixel detector is the innermost component of the CMS apparatus [1] at the LHC, with which a precise reconstruction of charged particles and secondary vertices from heavy quark decays will be performed. The barrel pixel detector (48 million pixels) consists of three cylindrical layers at radii of 4.4 cm, 7.4 and 10.2 cm, with a length of 53 cm. Four forward disks (18 million pixels) are located along the beam axis, two on each side (18 million pixels) at $\pm$34 cm and $\pm$47 cm from the collision point.

We were involved in the design, construction and commissioning of the barrel pixel detector. We have provided equipment and have led prototype tests on CERN beams [2, 3, 4], measuring sensor performances such as position resolution, detection efficiency, charge sharing and Lorentz deflection, before and after irradiation. We have also contributed to the development and commissioning of the readout chip (ROC) [5]. We have developed and built in the Institute workshop the mechanical and cooling structure and the two service tubes which provide the coolant and power, and transfer the signals to and from the pixel detector [6].

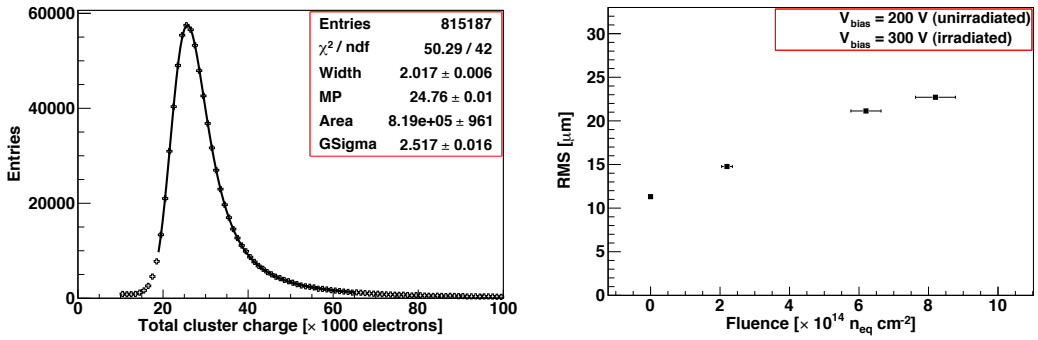

Figure 2.5: *Left: cluster charge distribution for the unirradiated sensor. The solid line is a Gaussian convoluted Landau fit. Right: position resolution as a function of irradiation fluence for perpendicular incidence (from [4]).*

In 2008 we continued the analysis of the test beam data taken in 2006. We had used a telescope with pixel sensors (150 μm $\times$ 100 μm pixels), two in front and two behind the irradiated pixel detector under test. Irradiated sensors were kept at -10°C in a cooling box with Peltier elements. The pixels were bump-bonded to the final CMS pixel readout chips. The apparatus was located in a Helmholtz superconductor 3T magnet and exposed to a 150 GeV π^--beam. The charge distribution of an unirradiated sensor operated at 150 V bias voltage in a 3T magnetic field is shown in fig. 2.5 (left). The solid line is the Gaussian convoluted Landau fit. The most probable value for the cluster charge is around 24'760 electrons. For irradiated pixels one observes a charge loss which is partially recovered by applying higher bias voltages. The collected charge is reduced to 77% (38%) for a fluence of 2.2×10^{14} (8.2×10^{14}) $\mathrm{n_{eq}cm^{-2}}$. The spatial resolution as a function of irradiation fluence is shown in fig. 2.5 (right). The degradation in the position resolution is due to charge loss as a result

of radiation damage. In addition, the higher bias voltage reduces the Lorentz angle, leading to reduced charge sharing among adjacent pixels.

We have developed reconstruction and physics analysis software, in particular track and vertex reconstruction [7, 8], and constraining kinematic fits [9]. This activity continues with the development of b-tagging algorithms [10]. We plan to exploit the first data from LHC for a study of $B_s \to J/\psi\ \phi$ [11, 12] and for a measurement of the $t\bar{t}$-cross section [13]. More information and related publications can be found in previous annual reports.

We are also preparing a search for supersymmetry in dijet events [14]. The study is focused on the SUSY parameter space where squarks are pair-produced and both decay into a quark and a neutralino. The latter escapes undetected and gives rise to missing energy. Although the background from QCD dijet events is overwhelming, powerful discriminating variables can be found due to the particular kinematics of SUSY events. This should enable results already with early collision data.

Figure 2.6: *One of the two racks of the UZH computing cluster. Visible are the 35 TeraByte storage RAID servers and three of the Linux servers, as well as some switching and cabling infrastructure.*

CMS (and the other LHC experiments) will produce enormous amounts of data to be processed and analyzed. This will be achieved by tiered computing architectures, dividing the data streams and processing tasks among several computing centers. The Tier-0 center is located directly at the experiment. A small number of Tier-1 centers perform the first steps of reprocessing. The skimmed data are accessible from Tier-2 centers (CSCS at Manno for us) and Tier-3 centers (PSI for us). The final stage of analysis is usually performed locally with small Tier-4 clusters, managed by the research groups themselves.

During 2008 we purchased and installed our own computing cluster at CERN. It consists of 28 CPU cores running at 3 GHz and 35 TeraByte of redundant (RAID) storage space, connected via a high-speed Fiber Channel Network. Efficient and easy access to all CERN services is available, since the whole cluster is located inside of the CERN network. Figure 2.6 shows a photograph of one of the two racks of the cluster. The computing nodes are running the Scientific Linux (SLC4) operating system, and the data storage is mounted on each computing node via the network file system (NFS). An air conditioning system was installed to provide the necessary cooling power to keep the room temperature well below 30 degrees. Uninterruptible power supplies prevent potential damage caused by the frequent power glitches and outages at CERN. Our computing cluster was already used for the cosmic runs in 2008.

We are responsible for the implementation, maintenance and validation of the barrel pixel geometry in the Monte-Carlo simulation. The description in the simulation [6] needs to be as precise as possible to reproduce the exact amount of material interactions. Such interactions deteriorate the trajectories of particles and influence the measurements in the outer detectors (strip tracker, calorimeters

and muon detectors). Figure 2.7 shows for example the material thickness in the CMS tracker as a function of pseudorapidity which reveals the relatively large thickness in the regions of pseudorapidity $1 < \eta < 1.5$. The weight of the pixel detector implemented in the Monte-Carlo simulation has been compared with its real weight and the agreement was found to be within 6%.

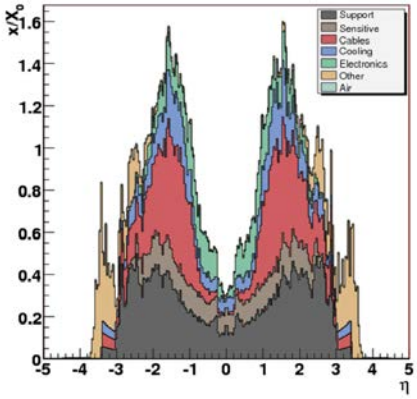

Figure 2.7: *Material thickness X (in radiation lengths X_0) in the CMS tracker, as a function of pseudorapidity η.*

The innermost layer of the pixel detector provides information on secondary vertices and impact parameters for b- and τ-decays which are relevant to Higgs searches. Studies of impact parameter resolution, track seeding, b- and τ-tagging efficiency will be performed. Before physics research can start, tasks such as software detector alignment and calibration need to be performed during the early phase of detector operation. Detector alignment, crucial for vertex reconstruction and b-tagging, is expected to improve with time and luminosity.

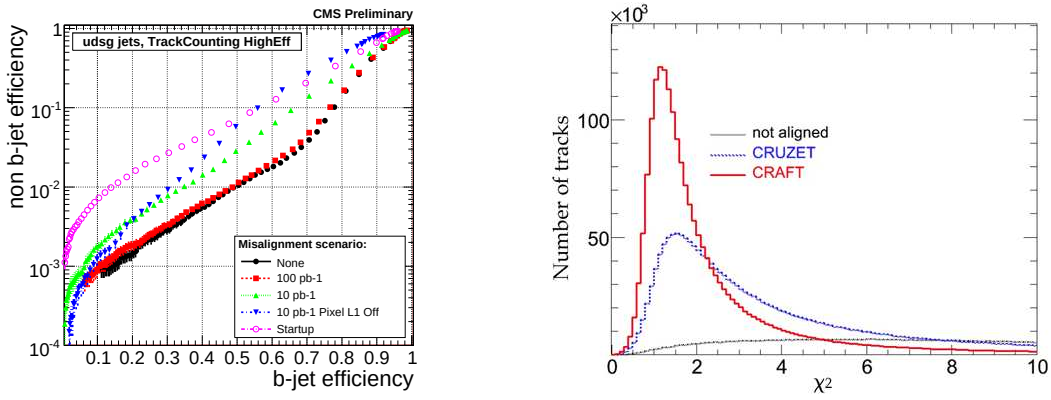

Figure 2.8: *Left: expected b-jet tagging efficiency vs. misidentification efficiency as a function of integrated luminosity, during which the detector alignment will be improved. Right: χ^2-distribution for reconstructed cosmic ray tracks, before and after alignment without magnetic field (CRUZET) and with magnetic field (CRAFT).*

We have simulated the expected efficiency of identifying b-jets ("b-tagging efficiency") for various degrees of detector alignment (fig. 2.8 , left). At startup only information from survey measurements and cosmic muon tracks can be used to perform the detector alignment. At 10 pb^{-1} the tracker can be aligned by using hadrons and muons from the decays of low mass resonances such as J/ψ and Υ. At 100 pb^{-1} high p_T muons from Z- and W-boson decays become available, at which time the misalignment of the pixel tracker is expected to be around 20μm. The tracker is finally aligned with

an integrated luminosity of 1 fb^{-1} which can be achieved within one year of detector operation.

The Monte-Carlo simulation then needs to be tuned according to detector performance. Large amounts of events need to be simulated using our Tier-3 facility at PSI. The simulation is time consuming (up to two minutes on a modern CPU and hundreds of millions of events are needed). A fast Monte-Carlo simulation is provided which uses parametrizations based on the full simulation and a simplified detector geometry [10, 15]. The fast simulation is 100 – 1000 $\times$ faster than the full simulation.

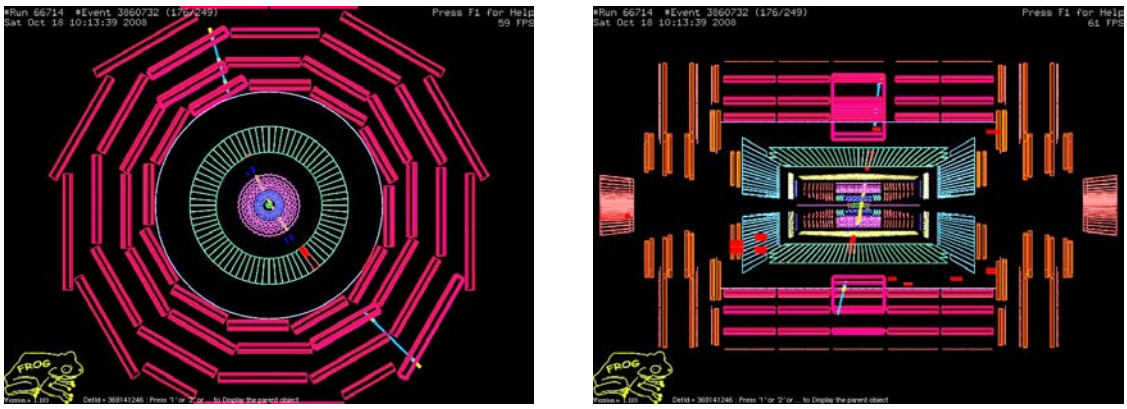

Figure 2.9: *A spectacular event display showing a cosmic muon crossing CMS and the pixel detector.*

The construction and installation of the pixel detector was completed in 2008 and operation started with beam on 10 September. Following the incident on 19 September, the detector was commissioned with cosmic ray data. Some 300 million events were collected until the end of the year. Data was taken without magnetic field ("CRUZET" data) and with 3.8 T ("CRAFT " data). With magnetic field turned on about 80'000 events had a muon crossing the pixel detector. Figure 2.9 shows one of the cosmic ray events. The various CMS subdetectors could be aligned with these data and the detection efficiencies measured. In particular, 99% (96%) of the barrel (forward) pixels was found to be operational.

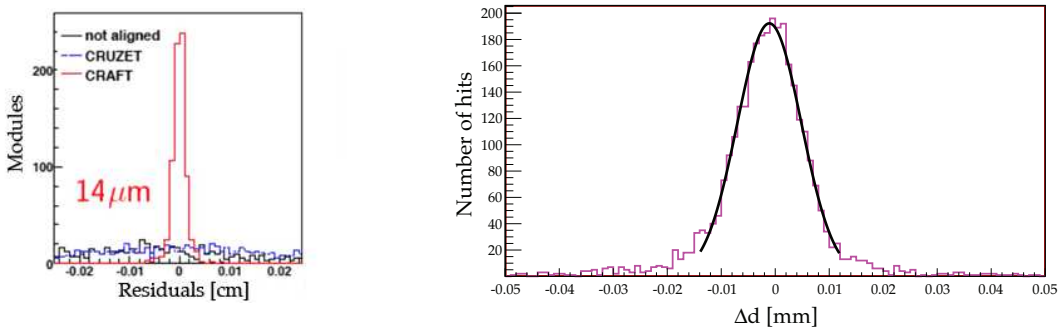

Figure 2.10: *Left: average residuals for the barrel pixels before and after alignment with cosmic rays with field off (blue) and field on (red). Right: Distribution of the difference Δd between the distances to the detector axis for the two half tracks originating from a high momentum cosmic muon.*

The tracking performance of the CMS detector depends crucially on the alignment of the tracking

devices, in particular of the pixel detector. Different alignment techniques are being used. In one method we use cosmic ray tracks traversing the pixel detector. For the pattern recognition this leads to two tracks emerging from the detector center. In a first step we use the outer strips from the tracker to determine the trajectories and to compute the difference (residuals) between the predicted and measured hits in the pixel detector. This is done for every sensor module. The average residual is then determined and used to align the detector. Figure 2.10 (left) shows the distribution of the average residuals for the barrel pixels before and after alignment. The accuracy on the alignment is around 14 μm r.m.s. Figure 2.10 (right) shows the difference of distances to the detector axis after detector alignment with cosmic rays of more than 20 GeV/c transverse momentum, which is a measure for the impact parameter resolution. The r.m.s resolution on the impact parameter is 59 $\pm$ 1 μm. Figure 2.8 (right) shows the spectacular improvement on the track reconstruction that could already be achieved with cosmics (described below). However, since cosmic rays are mostly vertical, the alignment of detectors lying in the horizontal plane will have to be performed with collision data.

Studying the differences between simulation and data helped to improve our understanding of the pixel detector. One of the most important variables is the cluster charge. Several effects have been identified which are not be reproduced in Monte-Carlo simulations, such as the dependence of the readout time on the signal amplitude. These effects have been studied extensively. Figure 2.11 (right) shows the cluster charge distribution after selection cuts, as measured with field on (CRAFT) in the barrel pixel detector. The simulation reproduces already quite well the peak-position and the measured width.

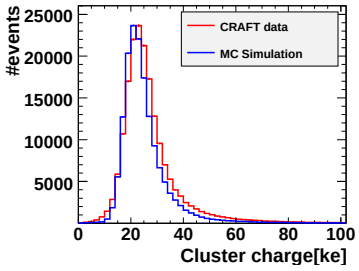

Figure 2.11: *Distribution of the cluster charge measured in the barrel pixel detector.*

In the 3.8 T field of CMS the electrons produced by a charged particle passing through the pixel detector drift perpendicularly to the magnetic and electric field in the sensor (fig. 2.12, left). This leads to a nonvanishing Lorenty angle θ_L and hence a shift of the hit coordinate. The correction (up to 120 μm) will decrease as a function of time. This is due to the increasing bias voltage needed to compensate for radiation damage (see below). Furthermore, since the irradiation is not uniform across the detector, each module will evolve differently. The Lorentz angle will therefore be estimated directly from data. With collision data this is done by comparing the observed shapes of charged clusters with the reconstructed tracks in the tracker [16].

Meanwhile we have determined θ_L from cosmic rays. The spread of the charge distribution over neighboring pixels depends on the particle incidence angle α and is minimum when the particle flies along the drift direction (when $\alpha = 90^\circ + \theta_L$, see fig. 2.12). Hence θ_L is measured by finding the minimum of the mean cluster size distribution, measured as a function of track incidence angle. The barrel pixel detector modules are perpendicular to the magnetic field while the forward modules are inclined by $\alpha = 20^\circ$ relative to the magnetic field, leading to in a much lower value θ_L for the forward detector. The results (fig. 2.12, right) are then compared to the PIXELAV simulation [17] of the pixel detector. The measured values agree well with the predicted values (see also table 2.1). Cosmic data

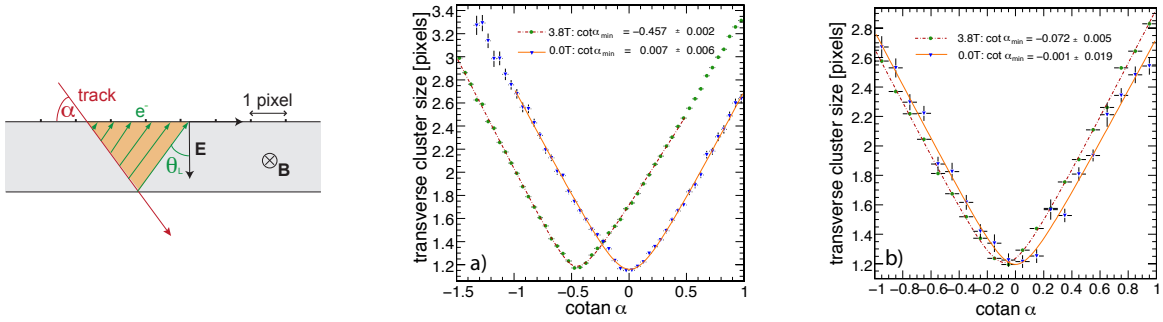

Figure 2.12: *Left: Lorentz angle θ_L. Right: measured cluster size as a function of incidence angle α for unirradiated pixels. The predictions (lines) are compared to data at 3.8 T (circles) and 0 T (triangles) for the barrel (a) and forward (b) pixel detector. Only statistical errors are shown (from [11]).*

	measured value ($\tan\theta_L$)	PIXELAV prediction ($\tan\theta_L$)
barrel	-0.4568 ± 0.0019	-0.452 ± 0.002
forward	-0.0718 ± 0.0046	-0.080 ± 0.005

Table 2.1: *Measured value for the Lorentz angle θ_L at 3.8 T for unirradiated pixels, compared with expectation for the barrel and forward pixel detectors.*

without magnetic field (for which $\theta_L = 0$) are used as a consistency check.

Operation with cosmic rays will resume in summer 2009 while first collisions with 10 TeV protons are expected in autumn.

References

[1] S. Chatrchyan *et al.* (CMS Collaboration), Journal of Instrumentation **3** (2008) S08004
[2] Y. Allkofer *et al.*, Nucl. Instr. Meth. in Phys. Research **A 584** (2008) 25
[3] V. Chiochia *et al.*, Nucl. Instr. Meth. in Phys. Research **A 568** (2006) 51;
V. Chiochia *et al.*, IEEE Trans. Nucl. Sci. **52** (2005) 1067
[4] E. Alagöz, PhD Thesis (in preparation)
[5] C. Hörmann, PhD Thesis, Universität Zürich (2006)
[6] C. Amsler *et al.*, submitted to Journal of Instrumentation
[7] R. Frühwirth and T. Speer, Nucl. Instr. and Meth. in Phys. Res. **A 534** (2004) 217
[8] R. Frühwirth, K. Prokofiev, T. Speer, P. Vanlaer and W. Waltenberger,
Nucl. Instr. Meth. in Phys. Res. **A 502** (2003) 699
[9] K. Prokofiev, PhD Thesis, Universität Zürich (2005)
[10] A. Schmidt, Nucl. Phys. B - Proceedings Supplements **187** (2009) 216
[11] L. Wilke, PhD Thesis (in preparation)
[12] B. Millan Mejias, PhD Thesis (in preparation)
[13] D. Tsirigkas, PhD Thesis (in preparation)
[14] T. Rommerskirchen, PhD Thesis (in preparation), CMS Note PAS SUS-08-005
[15] A. Schmidt, 2008 IEEE Nuclear Science Symposium Conference Record (2008) 2795
[16] L. Wilke, V. Chiochia, T. Speer, CMS Note 2008/012
[17] M. Swartz, Nucl. Instrum. Meth. **A 511** (2003) 88

3 Search for dark matter with liquid argon

C. Amsler, V. Boccone, W. Creus, A. Dell'Antone[2], S. Horikawa, P. Otyugova, C. Regenfus, and J. Rochet

In collaboration with:
ETHZ, CIEMAT (Madrid), Soltan Institute (Warsaw), Universities of Granada and Sheffield

(ArDM Collaboration)

Weak Interacting Massive Particles (WIMPs) are prime candidates for the dark matter in the universe [1]. Because dark matter has survived since the birth of the universe it has to be stable and only weakly interacting. The lightest supersymmetric particle in SUSY models conserving R-parity is the most popular candidate for WIMPs. This is the spin 1/2 neutralino χ with mass in the 10 GeV to 10 TeV range. R-parity conservation ensures that the χ is stable. Also, the χ cannot transform into other SUSY particles when interacting with matter, due to its low mass. At the LHC the χ will therefore manifest itself by a large missing energy. On the other hand, the χ can scatter e.g. on constituent quarks in nucleons or nuclei (fig. 3.13), leading to nuclear recoils in the range of 1 – 100 keV. Non-accelerator laboratory search experiments such as ArDM are all based on the detection of such nuclear recoils.

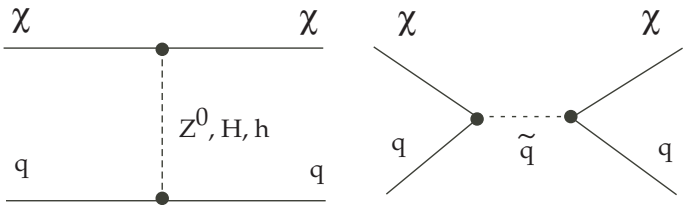

Figure 3.13: *Feynman graphs of χ interactions with quarks in the nucleon.*

The XENON-10 [2] and CDMS [3] experiments have produced the best upper limits so far of about 4×10^{-8} pb for the WIMP cross section on nucleons around WIMP masses of 30, resp. 70 GeV. We plan to improve on this upper limit for WIMPs by 1– 2 orders of magnitude and are constructing at CERN a 1t liquid argon detector using the two-phase technique to detect both charge and luminescence produced by the recoil nuclei following a WIMP interaction. Our experiment differs from other projects (e.g. [4]) by its large size and its measurement techniques. The Zurich group is studying ways to efficiently collect and detect the VUV light to reach a detection threshold of 30 keV in argon and to suppress background from neutrons and electrons, in particular from the β-emitter ^{39}Ar isotope.

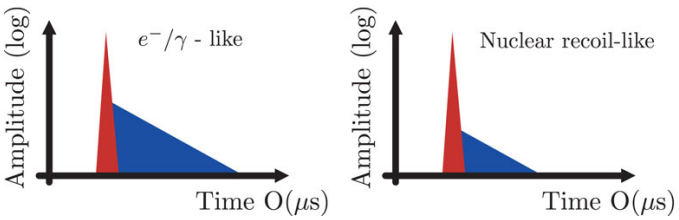

Figure 3.14: *Scintillation time distribution in pure argon for minimum ionizing particles (left) and nuclear recoils (right).*

Charged particles lead to ionization and excitation of argon atoms forming excimers (Ar_2^+ and Ar_2^*) with the lowest singlet and the triplet excited states decaying into the ground state (two independent atoms) by VUV photon emission in a narrow band around 128 nm. Reabsorption by argon atoms

[2]Visitor from Università degli Studi di Genova

is energetically suppressed. The singlet and the triplet states have different decay times, respectively $\tau_1 \simeq 7$ ns and $\tau_2 \simeq 1.6$ μs in liquid [5]. However, impurities such as water, air and CO_2 can absorb VUV light and reduce τ_2 [6, 7, 8]. The population ratio singlet/triplet depends on ionization density (fig. 3.14). For minimum ionizing projectiles such as *e* and γ the ratio is $\approx 1/2$, while for α's and nuclear recoils one finds a ratio of 4 – 5. Hence nuclear recoils from WIMPs populate mostly the fast decaying singlet state.

In addition, the ratio of scintillation to ionization yield is much higher for nuclear than for minimum ionizing particles. This is due to quick recombination which decreases the charge and enhances the luminescence. The higher ratio of light to charge production for nuclear recoils and the higher population of the fast decaying state can both be used to reduce background in WIMP searches.

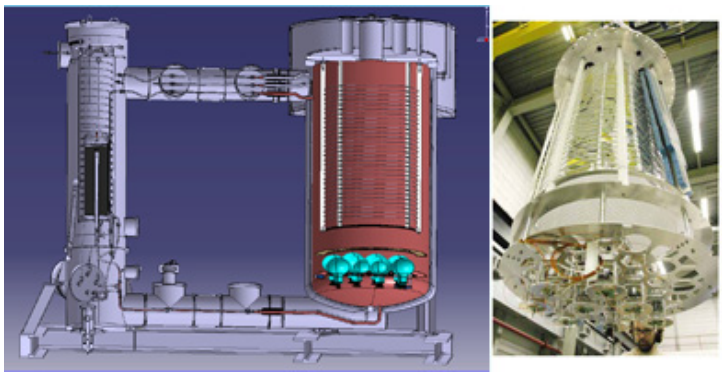

Figure 3.15: *Left: sketch of the ArDM detector and its purification system on the left. Right: Photograph of the detector showing the Greinacher HV divider, the WLS foils and the photomultiplier support mechanics.*

A sketch of the ArDM detector, as it is now installed in building 182 at CERN, is shown in fig. 3.15 (left). The working principle is as follows: in liquid argon a WIMP collision leading to 30 keV nuclear recoils produces about 400 VUV (128 nm) photons, together with a few free electrons. The latter are drifted in a strong vertical electric field and are detected in the gas phase by a large electron multiplier (LEM) above the surface of the liquid, while the VUV scintillation light from argon is shifted into blue light by a wavelength shifter (WLS) and detected by cryogenic photomultipliers at the bottom of the vessel. Fifteen Tetratex sheets (120 $\times$ 25 cm^2) are coated with WLS to cover the cylindrical walls inside the electric field shaping rings. The light detection system consists of fourteen 8" hemispherical photomultipliers (PMT, Hamamatsu R5912-MOD manufactured with Pt-underlays) at the bottom of the vessel. The PMT glass was coated with a thin WLS layer of a transparent tetraphenylbutadiene (TPB)-paraloid compound to increase the VUV light yield. The cryostat, the purification system, the Greinacher providing the 400 kV HV and the LEM are under the responsibility of ETHZ. Figure 3.15 (right) shows the detector inside the vessel. More details can be found in previous annual reports and in ref. [9].

In parallel to the construction of ArDM we continued R&D activities in our laboratory at CERN to measure and optimize the light output and collection efficiency for charged particles and neutron background [10]. Our aim is to achieve a detection efficiency of a few % (defined as the ratio of detected photoelectrons to emitted UV-photons) for the 128 nm fluorescence VUV-light generated in argon. An encouraging $\simeq 3\%$ in a test chamber with similar geometry as the 1t detector was achieved so far. The setup (fig. 3.16) is composed of two photomultipliers (Hamamatsu low temperature photomultipliers R6091-02MOD) facing an aluminum cylinder (height = 78 mm, diameter = 74 mm) containing liquid argon (fig. 3.16, right). A wavelength shifter (1mg/cm^2 of TPB [11]) was evaporated on the side reflectors. This time we chose Tyvek from DuPont as substrate for the wavelength shifter to allow a better mechanical stability than the Tetratex used before. The cell was softly baked and pumped for two weeks to reach a pressure of $5 \cdot 10^{-7}$ mbar.

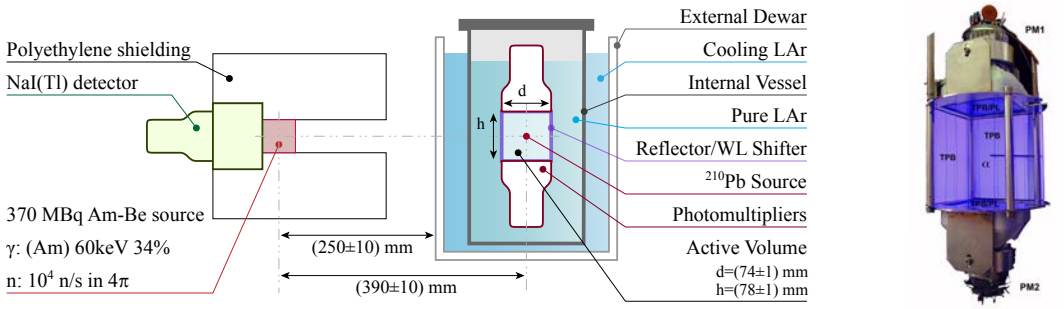

Figure 3.16: *Test cell to measure the light yield from various particles such as neutrons.*

A ^{210}Pb radioactive source was held on a metal stick in the middle of the active volume. Measurements with neutrons were obtained by placing a 370 MBq Am-Be source next to the experimental setup (fig. 3.16). The 5.4 MeV α's from americium are absorbed by beryllium producing 2 – 12 MeV neutrons (through the reaction ^{9}Be[α, n]^{12}C), 4.4 MeV γ's from the atomic level transition ^{12}C* $\rightarrow$^{12}C, and 60 keV photons from ^{241}Am decays. The source produced about 2·10^{4} n/s. It was contained in a high density polyethylene shielding block with two apertures, one for the neutrons, the second for the γ's to be detected in coincidence in a NaI(Tl) detector. The neutron flux at the target position was around 30 s^{-1}.

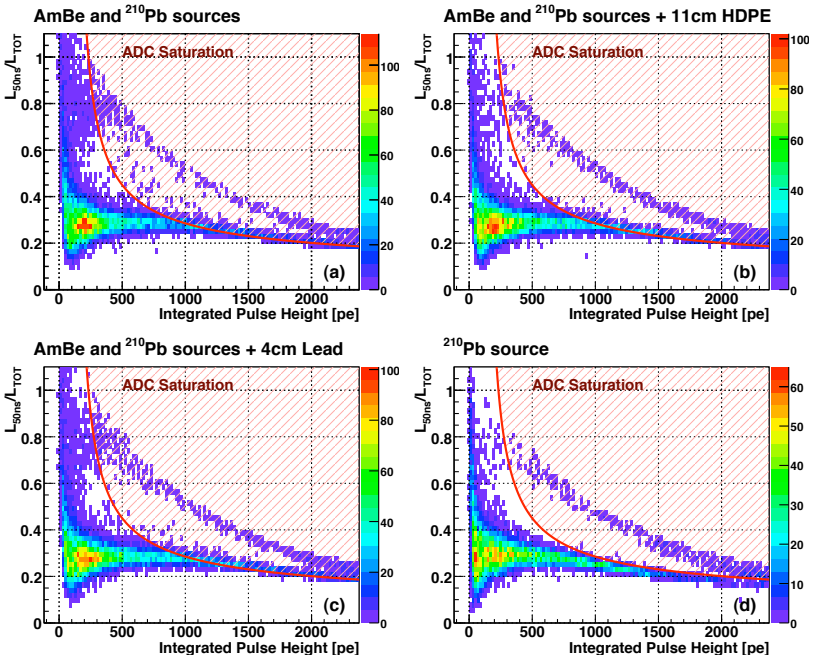

Figure 3.17: *Ratio $r = L_{50ns}/L_{TOT}$ of fast to total amplitude for the Am-Be- and Pb-sources (top left), for the Am-Be-source shielded with polyethylene (top right), and with 4 cm of lead (bottom left). The contribution from the Pb-source alone is shown in the bottom right figure.*

As pointed out before, heavily ionizing particles populate mostly the fast decaying singlet states. We therefore define the fraction r of fast ($<$ 50 ns) component to enhance nuclear recoils. The

signal from recoil nuclei associated with neutrons is shown in fig. 3.17 around r = 0.8. This can be proven by inserting a 11 cm thick polyethylene absorber, while a 4 cm lead sheet has no effect. The accumulation of events around $r = 0.3$ is due to recoil electrons, the diagonal band due to ADC saturation from α's.

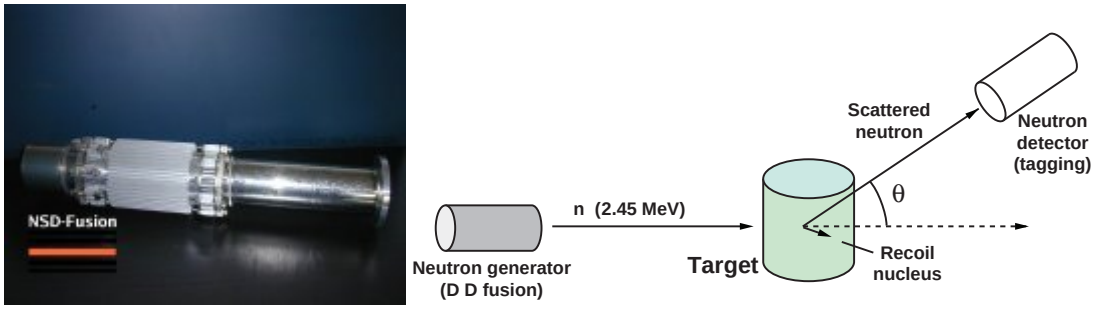

Figure 3.18: *Left: DD-neutron source. Right: neutron scattering experiment.*

Even small neutron fluxes around 1 MeV are potentially dangerous since the neutron-argon cross section is some 18 orders of magnitude larger than for WIMPs. It is therefore essential to investigate the response of the dark matter detector to neutrons as a function of recoil energy. A decisive advantage of monoenergetic neutrons over radioactive sources (such as Am-Be) is the known incident energy from which the energy transferred to the nucleus can be calculated by measuring the neutron elastic scattering angle.

We have therefore purchased a neutron source from NSD-Fusion GmbH (fig. 3.18, left). The source will deliver monoenergetic 2.45 MeV neutrons (10^7 s^{-1}) from the reaction DD $\rightarrow$ He^{3}n. A sketch of the experiment we intend to perform is shown in fig. 3.18 (right). The collimated neutrons are scattered by a small liquid argon cell and detected at a given angle θ by a liquid scintillator counter. We have estimated that, after collimation and using a 10 cm argon cell, we would obtain around 5 counts/s in the neutron detector. The purpose of the experiment is thus to measure the light yield as a function of nuclear recoil energy which differs strongly from that of electronic excitation, due to quenching.

In the 1t detector the probability for two or more neutron interactions is large enough to be measured precisely. This fraction can be measured with the DD-source and used to reduce the neutron background during WIMP searches, since WIMP interactions do not lead to multiple scattering events.

During 2008 the design of the DD-source was optimised in collaboration with the producer to fulfil the safety and radiation requirements at CERN, so that the source could be operated in our laboratory close to our offices. We had also to provide our own GEANT4 simulation of the expected radiation levels in and around our laboratory (fig. 3.19). The apparatus includes a real time ambient neutron dose monitoring system, and components for an operation interlock. A safety fence will be installed to avoid access to the radiation area during operation.

The neutron source, including its 27 mm thick aluminium housing, is surrounded by a 1 m long cylindrical shielding (50 cm of polyethylene). A hole, 10 cm in diameter, provides the collimated beam of neutrons. The neutron energy spectrum of the neutrons exiting the collimator is shown in fig. 3.19, bottom. About 1.5% of the total neutron flux reaches the argon cell located at 1 m of the source. A fraction of 20% of the neutrons have the initial energy of 2.45 MeV, while 60% are thermalized.

Meanwhile we have purchased a liquid scintillator cell from SCIONIX with a photomultiplier

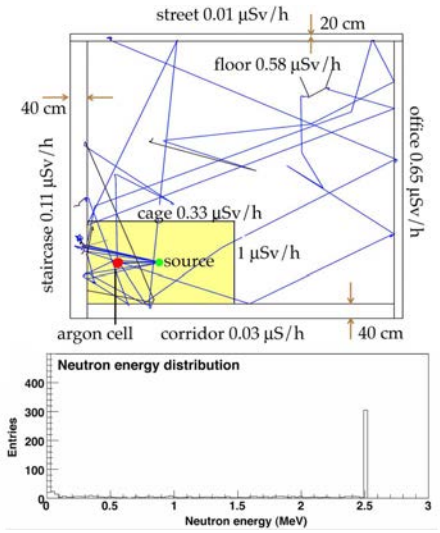

Figure 3.19: *Top: predicted dose distribution in our laboratory with the neutron source in operation (the tolerated radiation dose is 2.5 µSv/h). The rays are typical neutron trajectories. Bottom: energy spectrum of neutrons at the argon cell.*

coupled to a 3" × 3" cell filled with $C_6H_4(CH_3)_2$, which has a high H:C ratio of 1.21 (fig. 3.20, left). This kind of detector is applicable for neutrons above 50 keV and gives information on the neutron energy, since the recoil proton is fully absorbed in the cell. Neutrons can also be separated from γ-events by pulse shape discrimination. Figure 3.20 shows preliminary measurements with the Am-Be-source, displaying the normalized and averaged pulse shapes from electron and proton recoils, and the discrimination power between neutrons and photons.

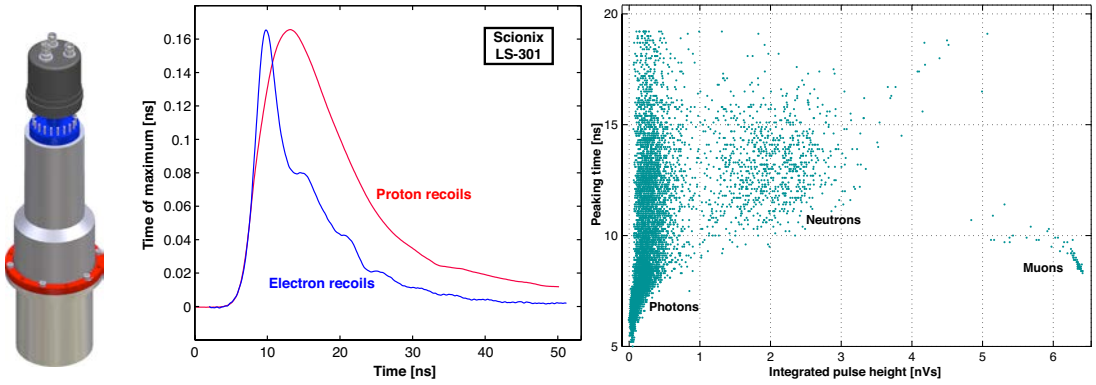

Figure 3.20: *Left: SCIONIX liquid scintillator cell. Middle: normalized pulse shape from electron and proton recoils. Right: peak-time vs. integrated pulse height measured with the Am-Be source.*

As mentioned before, the purity in argon (and therefore the scintillation quality) can be monitored by measuring the lifetime of the slow component [6]. We have therefore built another small liquid argon cell connected to the 1t detector (fig. 3.21). A 10 Bq ^{210}Pb source for the argon excitation is used to monitor the lifetime of the slow component every 10 s. We use a small Hamamatsu R8486 PMT with MgF_2 window and CsTe photocathode which is directly sensitive to 128 μm VUV-photons (quantum efficiency 20%) and therefore does not require a WLS. The device (56 mm in diameter and 50 cm high) is rather compact.

The ArDM detector becomes operational in 2009 and will hopefully be moved to an underground location in 2011, following the extensive performance tests which can be most conveniently per-

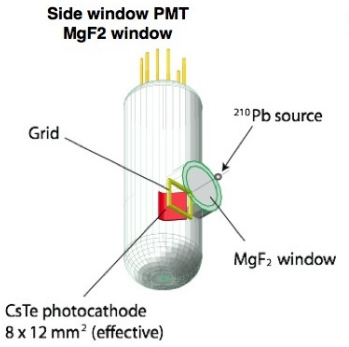

Figure 3.21: *Sketch of the liquid argon purity monitor. A small PMT with VUV sensitive photocathode and a ^{210}Pb-source emitting both α and β are immersed in liquid argon.*

formed on the surface at CERN.

References

[1] For a reviews on dark matter searches see M. Drees and G. Gerbier, Phys. Lett. **B 667** (2008) 1
[2] J. Angle *et al.*, (XENON-10 collaboration), Phys. Rev. Lett. **100** (2008) 021303
[3] Z. Ahmed *et al.* (CDMS collaboration), Phys. Rev. Lett. **102** (2009) 011301
[4] N. Ferrari *et al.*, (WARP collaboration), J. Phys. Conf. Ser. **39** (2006) 111
[5] A. Hitachi *et al.*, Phys. Rev. **B 27** (1983) 5279
[6] C. Amsler *et al.*, Journal of Instrumentation **3** (2008) P02001
[7] A. Büchler, Bachelor Thesis, Universität Zürich (2006)
[8] M. Thomann, Bachelor Thesis, Universität Zürich (2008)
[9] V. Boccone, PhD thesis, Universität Zürich, in preparation: V. Boccone, Proc. XIII Int. Conf. on Calorimetry in High Energy Physics, Pavia (2008), prep. arXiv:0810.4490v1
[10] V. Boccone *et al.* (ArDM Collaboration) prep. arXiv:0904.0246v1, submitted to Journal of Instrumentation
[11] H. Cabrera, Master Thesis, Universität Zürich (2007)

4 Publications

Articles

1. A new aerogel Cherenkov detector for DIRAC-II
   Y. Allkofer et al.
   Nucl. Instrum. Meth. in Phys. Research **A 595** (2008) 84

2. The C_4F_{10} Cherenkov detector for DIRAC-II
   S. Horikawa et al.
   Nucl. Instrum. Meth. in Phys. Research **A 595** (2008) 212

3. Evidence for πK-atoms with DIRAC
   B. Adeva et al. (DIRAC Collaboration)
   Physics Letters **B 674** (2009) 11

4. Review of Particle Physics
   C. Amsler et al. (Particle Data Group)
   Physics Letters **B 667** (2008) 1

5. Temporally Controlled Modulation of Antihydrogen Production and the Temperature Scaling of Antiproton-Positron Recombination
   M.C. Fujiwara et al. (ATHENA Collaboration)
   Phys. Rev. Lett. **101** (2008) 053401

6. The CMS experiment at the CERN LHC
   S. Chatrchyan et al. (CMS Collaboration)
   Journal of Instrumentation **3** (2008) S08004

7. The $\eta(1405)$, $\eta(1475)$, $f_1(1420)$, and $f_1(1510)$
   C. Amsler and A. Masoni
   Phys. Lett. **B 667** (2008) 641

8. Note on scalar mesons
   N.A. Törnqvist, S. Spanier and C. Amsler
   Phys. Lett. **B 667** (2008) 594

9. Quark Model
   C. Amsler, T. DeGrand and B. Krusche
   Phys. Lett. **B 667** (2008) 172

10. Search for πK-atoms with DIRAC
    Y. Allkofer
    Inaugural Dissertation, Universität Zürich, 2008

11. 2008 Particle Physics Booklet
    C. Amsler et al. (Particle Data Group)
    Special issue printed by Elsevier

12. Low energy tracking and particles identification in the MUNU Time Projection Chamber at 1 bar: possible application in low energy solar neutrino spectroscopy.
    Z. Daraktchieva et al. (MUNU Collaboration)
    J. Phys. G: Nucl. Part. Phys. **35** (2008) 125107

13. B physics at CMS
    T. Speer
    Proc. 2007 Eur. Conf. on High Energy Physics, Manchester
    Journal of Physics: Conference Series **110** (2008) 052049

14. Beauty Production and Identification at CMS
    A. Schmidt
    Nuclear Physics B (Proceedings Supplements) **187** (2009) 216

15. Search for πK-atoms with DIRAC II
    Y. Allkofer et al.
    Proc. XII Int. Conf. on Hadron Spectroscopy
    Physics Series, Vol. **XLVI** (2008) 883

16. Fast Simulation of the CMS Detector at the LHC
    A. Schmidt
    IEEE NUckear Science Symposium Conference Record **N37-4** (2008) 2795

17. A novel technique for the reconstruction and simulation of hits in the CMS Pixel Detector
    V. Chiochia
    IEEE NUckear Science Symposium Conference Record **N27-3** (2008) 1909

Notes/Reports

1. Impact of Tracker Misalignment on the CMS b-tagging performance
   A. Schmidt et al.
   CMS Note AN-2007/047

2. SUSY searches with dijet events
   T. Rommerskirchen and the CMS collaboration
   CMS Physics analysis report SUS-08-005

3. Beauty Production and Identification at CMS
   A. Schmidt
   CMS Conference report CR-2008/061

4. Gamma ray bursts : observation and theoretical conjectures
   E. Alagöz et al.
   CERN Yellow report 2008-004 (2008) 287

Articles in press

1. Development of wavelength shifter coated reflectors for the ArDM argon dark matter detector
   V. Boccone et al. (ArDM Collaboration)
   Journal of Instrumentation (2008)

2. Mechanical Design and Material Budget of the CMS Barrel Pixel Detector
   C. Amsler et al.
   Journal of Instrumentation (2008)

3. Position resolution for the CMS Barrel Pixel Detector after irradiation
   E. Alagöz
   Proc. 11th Topical Seminar on Innovative Particle and Radiation Detectors, Siena, 2008
   Nucl. Phys. B

4. The ArDM project: A Liquid Argon TPC for Dark Matter Detection
   V. Boccone
   Proc. XIII Int. Conf. on Calorimetry in High Energy Physics (CALOR 08), Pavia, 2008
   Prep. arXiv:0810.4490v1, Journal of Physics

5. Experience with CMS pixel software commissioning
   V. Chiochia
   Proc. 17th Int. Workshop on Vertex detectors (Vertex 08), Stockholm, 2008
   Prep. arXiv:0812.0681, Proceedings of Science

6. Observation of πK-atoms with DIRAC-II
   Y. Allkofer
   Int. conf. on exotic atoms and related topics (EXA08), Vienna, 2008
   Hyperfine Interactions

7. Searches for New Phenomena at CMS and ATLAS
   T. Rommerskirchen
   Moriond QCD and High Energy Interactions, La Thuile, 2009

8. Heavy Flavour Physics et CMS and ATLAS
   L. Wilke
   Moriond QCD and High Energy Interactions, La Thuile, 2009

Invited Lectures

1. E. Alagöz
   Proc. 11th Topical Seminar on Innovative Particle and Radiation Detectors, Siena
   3 October 2008
   "Position resolution for the CMS Barrel Pixel Detector after irradiation"

2. Y. Allkofer
   Int. conf. on exotic atoms and related topics (EXA08), Vienna
   15 September 2008
   "Observation of πK-atoms with DIRAC-II"

3. C.Amsler
   Physik-Kolloquium, Universität Basel
   20 February 2009
   "From Antihydrogen to Dark Matter, Experimental Challenges"

4. V. Boccone
   Proc. XIII Int. Conf. on Calorimetry in High Energy Physics (CALOR 08), Pavia
   28 May 2008
   "The ArDM project: A Liquid Argon TPC for Dark Matter"

5. V. Chiochia
   Proc. 17th Int. Workshop on Vertex detectors (Vertex 08), Stockholm
   27 July 2008
   "Experience with CMS pixel software commissioning"

6. V. Chiochia
   IEEE Nuclear Science Symposium, Dresden
   19 October 2008
   "A novel technique for the reconstruction and simulation of hits in the CMS Pixel Detector"

7. P. Otyugova
   3rd CHIPP Neutrino Meeting, Zurich
   17 November 2008
   "The ArDM - 1 ton Experiment"

8. C. Regenfus
   4th Patras Workshop on Axions, WIMPs and WISPs, DESY, Hamburg
   19 June 2008
   "The Argon Dark Matter Experiment (ArDM)"

9. T. Rommerskirchen
   Moriond QCD and High Energy Interactions 2009, La Thuile
   17 March 2009
   "Searches for New Phenomena at CMS and ATLAS"

10. A. Schmidt
    IEEE Nuclear Science Symposium, Dresden
    20 October 2008
    "Fast Simulation of the CMS Detector at the LHC"

11. A. Schmidt
    Eighth Int. Conf. on Hyperons, Charm and Beauty Hadrons (BEACH2008), Columbia, USA
    22 June 2008
    "Beauty Production and Identification at CMS"

12. L. Wilke
    Meeting of the Swiss Institute of Particle Physics (CHIPP), Lausanne
    8 September 2008
    "LHC status and upgrade plan: CMS"

13. L. Wilke
    Moriond QCD and High Energy Interactions 2009, La Thuile
    16 March 2009
    "Heavy Flavour Physics et CMS and ATLAS"

ArDM Collaboration (2008):
C. Amsler, A. Badertscher, V. Boccone, A. Bueno, H. Cabrera, M. C. Carmona-Benitez, M. Daniel , E. J. Daw, U. Degundab, A. Dell'Antone, A. Gendotti, L. Epprecht, S. Horikawa, L. Kaufmann, L. Knecht, M. Laffranchi, C. Lazzaro, P. K. Lightfoot, D. Lussi, J. Lozano, A. Marchionni, K. Mavrokoridis, A. Melgarejo, P. Mijakowski, G. Natterer, S. Navas-Concha, P. Otyugova, M. de Prado, P. Przewlocki

, C. Regenfus, F. Resnati, M. Robinson, J. Rochet, L. Romero , E. Rondio, A. Rubbia, N. J. C. Spooner, T. Strauss, J. Ulbrichtb, T. Viant.

ATHENA Collaboration (2008):
M. Amoretti, C. Amsler, G. Bonomi, C. Carraro, C. L. Cesar, M. Charlton, M. Doser, A. Fontana, R. Funakoshi, P. Genova, R. S. Hayano, L. V. Joergensen, A. Kellerbauer, V. Lagomarsino, R. Landua, E. Lodi Rizzini, M. Macri, N. Madsen, G. Manuzio, D. Mitchard, P. Montagna, L. G. Posada, H. Pruys, C. Regenfus, J. Rochet, A. Rotondi, G. Testera, D. P. Van der Werf, A. Variola, L. Venturelli, Y. Yamazaki, N. Zurlo.

DIRAC Collaboration (2008):
B. Adeva, L. Afanasyev, Y. Allkofer, C. Amsler, A. Anania, A. Benelli, V. Brekhovskikh, G. Caragheorgheopol, T. Cechak, M. Chiba, P. Chliapnikov, C. Ciocarlan, S. Constantinescu, C. Curceanu, C. Detraz, D. Dreossi, D. Drijard, A. Dudarev, M. Duma, D. Dumitriu, J.L. Fungueiriño, J. Gerndt, A. Gorin, O. Gorchakov, K. Gritsay, C. Guaraldo, M. Gugiu, M. Hansroul, Z. Hons, S. Horikawa, M. Iliescu, V. Karpukhin, J. Kluson, M. Kobayashi, V. Komarov, V. Kruglov, L. Kruglova, A. Kulikov, A. Kuptsov, I. Kurochkin, K.-I. Kuroda, A. Lamberto, A. Lanaro, V. Lapshin, R. Lednicky, P. Levi Sandri, A. Lopez Aguera, V. Lucherini, I. Manuilov, C. Mariñas, L. Nemenov, M. Nikitin, K. Okada, V. Olchevskii, M. Pentia, A. Penzo, M. Pló, G.F. Rappazzo, C. Regenfus, J. Rochet, A. Romero, V. Ronjin, A. Ryazantsev, V. Rykalin, J. Saborido, J. Schacher, A. Sidorov, J. Smolik, S. Sugimoto, F. Takeutchi, A. Tarasov, L. Tauscher, T. Trojek, S. Trusov, V. Utkin, O. Vázquez Doce, T. Vrba, V. Yazkov, Y. Yoshimura, M. Zhabitsky, P. Zrelov.

PARTICLE DATA Group (2008):
C. Amsler, M. Doser, M. Antonelli, D. Asner, K.S. Babu, H. Baer, H.R. Band, R.M. Barnett, J. Beringer, E. Bergren, G. Bernardi, W. Bertl, H. Bichsel, O. Biebel, P. Bloch, E. Blucher, S. Blusk, R.N. Cahn, M. Carena, 1 C. Caso, A. Ceccucci, D. Chakraborty, M.-C. Chen, R.S. Chivukula, G. Cowan, O. Dahl, G. D'Ambrosio, T. Damour, A. de Gouvea, T. DeGrand, B. Dobrescu, M. Drees, A. Edwards, S. Eidelman, V.D. Elvira, J. Erler, V.V. Ezhela, J.L. Feng, W. Fetscher, B.D. Fields, B. Foster, T.K. Gaisser, L. Garren, H.-J. Gerber, G. Gerbier, T. Gherghetta, G.F. Giudice, M. Goodman, C. Grab, A.V. Gritsan, J.-F. Grivaz, D.E. Groom, M. Grnewald, A. Gurtu, T. Gutsche, H.E. Haber, K. Hagiwara, C. Hagmann, K.G. Hayes, J.J. Hernndez-Rey, K. Hikasa, I. Hinchliffe, A. Hcker, J. Huston, P. Igo-Kemenes, J.D. Jackson, K.F. Johnson, T. Junk, D. Karlen, B. Kayser, D. Kirkby, S.R. Klein, I.G. Knowles, C. Kolda, R.V. Kowalewski, P. Kreitz, B. Krusche, Yu.V. Kuyanov, Y. Kwon, O. Lahav, P. Langacker, A. Liddle, Z. Ligeti, C.-J. Lin, T.M. Liss, L. Littenberg, J.C. Liu, K.S. Lugovsky, S.B. Lugovsky, H. Mahlke, M.L. Mangano, T. Mannel, A.V. Manohar, W.J. Marciano, A.D. Martin, A. Masoni, D. Milstead, R. Miquel, K. Mnig, H. Murayama, K. Nakamura, M. Narain, P. Nason, S. Navas, P. Nevski, Y. Nir, K.A. Olive, L. Pape, C. Patrignani, J.A. Peacock, A. Piepke, G. Punzi, A. Quadt, , S. Raby, G. Raffelt, B. Renk, P. Richardson, S. Roesler, S. Rolli, A. Romaniouk, L.J. Rosenberg, J.L. Rosner, C.T. Sachrajda, Y. Sakai, S. Sarkar, F. Sauli, O. Schneider, D. Scott, B. Seligman, M. Shaevitz, T. Sjstrand, J.G. Smith, G.F. Smoot, S. Spanier, H. Spieler, A. Stahl, T. Stanev, S.L. Stone, T. Sumiyoshi, M. Tanabashi, J. Terning, M. Titov, N.P. Tkachenko, N.A. Trnqvist, D. Tovey, G.H. Trilling, T.G. Trippe, G. Valencia, K. van Bibber, M.G. Vincter, P. Vogel, D.R. Ward, T. Watari, B.R. Webber, G. Weiglein, J.D. Wells, M. Whalley, A. Wheeler, C.G. Wohl, L. Wolfenstein, J. Womersley, C.L. Woody, R.L. Workman, A. Yamamoto, W. -M. Yao, O.V. Zenin, J. Zhang, R.-Y. Zhu P.A. Zyla.